Available online at www.sciencedirect.com
SCIENCE DIRECT®
Physica B 336 (2003) 162–172
PHYSICA B
www.elsevier.com/locate/physb

Distribution of vortices in Nb/Al multilayers studied by spin-polarized neutron reflectivity and magnetization

S.-W. Han[a,1], J. Farmer[b], P.F. Miceli[a,*], G. Felcher[c], R. Goyette[c], G.T. Kiehne[d], J.B. Ketterson[d]

[a] *Department of Physics and Astronomy, University of Missouri-Columbia, Columbia, MO 65211, USA*
[b] *Missouri University Research Reactor, Columbia, MO 65211, USA*
[c] *Material Science Division, Argonne National Laboratory, Argonne, IL 60439, USA*
[d] *Department of Physics and Astronomy and the Materials Research Center, Northwestern University, Evanston, IL 60208, USA*

Received 23 November 2002; accepted 27 February 2003

Abstract

We present SPNR and DC magnetization studies of non-uniformly distributed vortices in Nb/Al multilayers for fields applied near-parallel to the film surface. Peaks are observed in the *M–H* curves that are shown to correspond to vortex row-transitions and the field values of the transitions agree well with free energy calculations. An additional peak is observed at an applied field smaller than the first row-transition field and this is shown to arise from the lower critical field parallel to the surface. Demagnetization effects are discussed. SPNR measurements performed at low field give the London penetration length and measurements in the mixed state are consistent with a single row of vortices residing in the film center, but with positional fluctuations amounting to 1/4 of the film thickness. It is also shown that cycling the applied field leads to a surface-induced reorientation of the vortex magnetic field, which points perpendicular to the surface in zero field.

PACS: 74.60.Ge; 61.12.Ha; 74.25.Ha

Keywords: SPNR; Spin-polarized neutron reflectivity; Nb/Al multilayers, Superconductivity

1. Introduction

Magnetic vortices in a type-II superconductor not only feel a mutual repulsion that usually leads to an ordered vortex lattice, but the vortices also feel the effects of the surface where the Bean–Livingston surface barrier [1,2] can significantly influence the motion of vortices into and out of the superconductor. When a field is applied parallel to the surface of a thin film having a thickness, t, that is comparable to the London penetration length, the interaction of vortices with the surface is particularly strong. In this case, there is substantial experimental and theoretical evidence for the surface-induced ordering of vortices into rows

*Corresponding author.
E-mail address: micelip@missouri.edu (P.F. Miceli).
[1] Present address: Chemical Sciences Division, Lawrence Berkeley National Laboratory, Berkeley, CA 94720, USA.

0921-4526/03/$ - see front matter © 2003 Elsevier Science B.V. All rights reserved.
doi:10.1016/S0921-4526(03)00286-2

that are parallel to the surface [3,4]: just above H_{c1}, the vortices reside within a single row in the center of the film and there are transitions to two or more rows as the applied field is increased. Experimental studies of these systems have used macroscopic probes, including magnetization [3,9,4], electron tunneling [5], microwave absorption [6], resistivity [7], superconducting channel device [8], and internal friction [10,11]. Of course, these techniques measure only the average magnetization or the effects of vortex motions and it would be useful to have a microscopic probe that could directly investigate the ordered structure itself.

Spin-polarized neutron reflectivity (SPNR) can detect the spatial variation of magnetic fields on a microscopic scale and it has been employed in studies of superconducting thin films to determine the London penetration length, λ_L, at low applied field [12]. At higher applied field, the quantitative sensitivity of SPNR to vortices has been recently demonstrated [13–15]. Lauter–Pasyuk et al. have used SPNR to observe the vortex row-transitions in a film of $YBa_2Cu_3O_{7-x}$ with $t \sim 2\lambda_L$ [14]. Han et al. have observed a surface-induced reorientation of the vortex magnetic field in a Nb film with $t \sim 3\lambda_L$ [15].

In this paper, we report our initial SPNR and magnetization measurements of Nb/Al multilayers, which is a system that should allow a detailed investigation into surface-induced effects on vortices in thin-films, including their reorientation, ordering and phase diagram. The experimental details are given in Section 2 and the SPNR results are discussed in Section 3, while the magnetization model and measurements are presented in Sections 4 and 5, respectively.

2. Experimental details

Three multilayer samples were fabricated by depositing bilayers of Nb/Al (Nb(72 Å)/Al(20 Å), Nb(100 Å)/Al(20 Å) or Nb(130 Å)/Al(20 Å)), repeated 20 times, onto Si substrates by direct-current sputtering with an Ar partial pressure of 5 mTorr in a chamber having a base pressure of $\sim 10^{-4}$ mTorr. During the deposition, the power was applied to a Nb target with 275 W (297 V) and an Al target with 200 W (372 V) from which the deposition rate was 5.9 Å/s for Nb and 4.7 Å/s for Al while the substrate was held at the ambient temperature. A top layer of Nb was deposited to protect the multilayer. $T_c = 7.25 \pm 0.25$ K, for the Nb(72 Å)/Al(20 Å) multilayer, was determined by magnetization measurement at an applied field 50 Oe.

For the magnetization measurements, the samples were mounted on an extended sample holder placed in a cryostat so that the film surface was near-parallel to the applied field of the SQUID magnetometer. The samples were zero-field cooled. The tilt angle between the surface and applied field was controlled by shimming non-magnetic plastic pieces between the sample holder and sample. The tilt angle was reproducible within $\pm 0.25^\circ$.

SPNR measurements from the Nb(72 Å)/Al(20 Å) multilayer were performed at the POSY1 reflectometer at the intense pulsed neutron source which is located at Argonne National Laboratory. The specimen was zero-field-cooled in a pumped-He cryostat and a magnetic field was applied parallel to the film surface where the tilt angle was less than 0.5 degree. Polarized neutrons parallel ("spin-up") or anti-parallel ("spin-down") were reflected from the sample at a fixed incident angle 0.45 degree and the reflected beam was not polarization analyzed.

The data were modeled by solving Schrödinger's equation for each spin state using a neutron potential that varies along the direction perpendicular to the sample surface, $V(z) = 2\pi\hbar^2 n(z)b(z)/m_n \mp \mu_n M(z)$, where "–" corresponds to spin-up and "+" to spin-down, m_n is the neutron mass and μ_n is the neutron magnetic moment. Because of the condition of specular reflection, quantities in the potential are averaged in the plane of the film and vary only in the direction perpendicular to the surface. $n(z)b(z)$ is nuclear scattering length density and $M(z)$ is the spatially varying sample magnetization. Corrections for the polarization efficiency $\sim 97\%$ and the instrumental resolution $\Delta q/q = 0.053$ were included in the analysis of the reflectivity data.

Although we will discuss the magnetization studies in more detail in Section 5, here we present

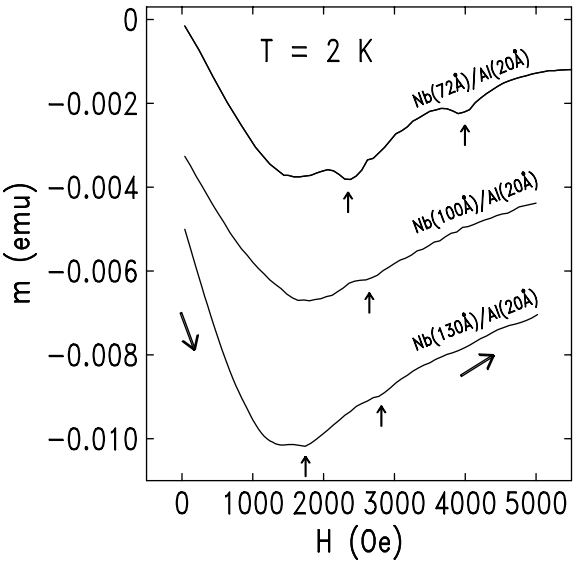

Fig. 1. Magnetization measured from Nb/Al multilayers at 2 K. The data of Nb(100 Å)/A1(20 Å) and Nb(130 Å)/A1(20 Å) were shifted vertically along -m for clarity. The small arrows indicate the peak positions and the big arrows show the direction of the field change.

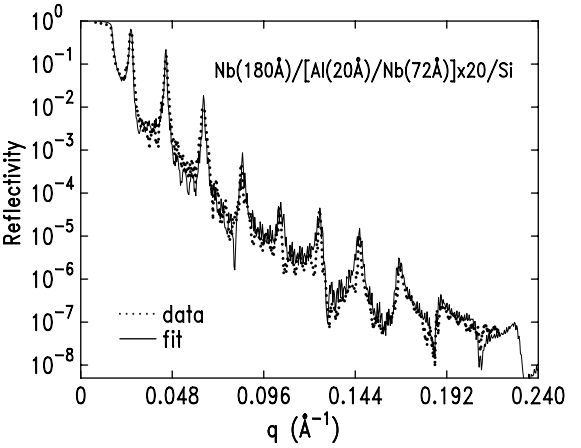

Fig. 2. X-ray reflectivity measured from the Nb(72 Å)/Al(20 Å) multilayer at ambient. The dotted line is the data and the solid line is a best fit.

a brief overview that motivates the SPNR measurement. Fig. 1 shows the ascending-field magnetization measured for each of the samples of 2 K with the applied field parallel to the surface. The magnetization reveals small peaks (indicated by vertical arrows), similar to those associated with vortex-ordering transitions in Nb/Cu multilayers. By analogy, the first magnetization peak (observed here at 2250 Oe) corresponds to a transition from a single-row of vortices to a double-row of vortices. The peak positions in Fig. 1 are found to depend on the thickness of the Nb layer and the magnitude of the magnetization anomally decreases with increasing thickness. Because the peaks are largest for the Nb(72 Å)/Al(20 Å) multilayer, that sample was chosen for the SPNR measurements, reported below.

In order to characterize the interfaces of the Nb(72 Å)/Al(20 Å) multilayer, the X-ray specular reflectivity was measured as a function of wavevector, q, at room temperature (see Fig. 2). The data were modeled using a variation of Parratt's method that includes a cumulative Gaussian roughness at each interface [16]. A best fit (solid line) gives thicknesses according to Nb(120 ± 20 Å)/[Al(19 ± 1.5 Å)/Nb(74.5 ± 2.5 Å)] × 20/Si and the rms roughness at the air/Nb interface is ~15 Å while the roughness of the Si substrate is ~2.2 Å. Each Nb layer has the roughness ~6 Å and each Al layer has a roughness ~2.5 Å. A slight improvement of the fit was achieved by including an extra layer at the air/Nb interface with thickness ~60 Å and an X-ray scattering density half that of Nb. The origin of this layer is not clear, although, we speculate that it might compensate for a non-Gaussian roughness at the air/Nb interface.

3. SPNR measurements

SPNR measurements were performed on the Nb[72 Å]/Al[20 Å] multilayer to investigate the density and distribution of vortices which run parallel to the surface. A measurement was first performed at a low applied field in order to determine the London penetration length for the sample. Fig. 3(a) shows neutron specular reflectivities measured as a function of q for spin-up and spin-down neutrons at 700 Oe and 2 K. The oscillation period corresponds to the total film thickness of ~2020 Å. A best fit (solid line) to the

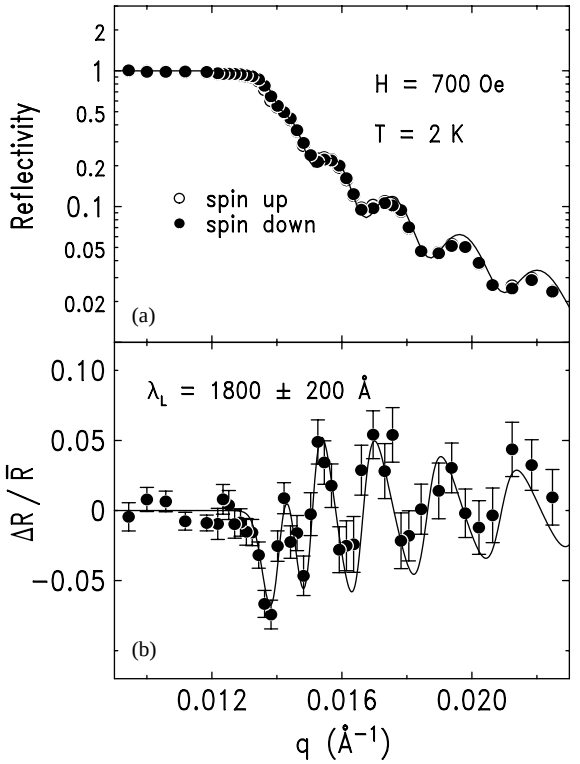

Fig. 3. (a) shows the reflectivities for spin-up and spin-down neutrons from a Nb(72 Å)/Al(20 Å) multilayer measured as a function of q at 700 Oe and 2 K. The solid line is a best fit. (b) shows $\Delta R/\bar{R}$ obtained from the data in (a). The solid line is a best fit that gives $\lambda_L \sim 1800$ Å for the multilayer.

structural model gives a top Nb layer thickness of 180 ± 40 Å and the multilayer thicknesses are $[\mathrm{Al}(20 \pm 2\,\text{Å})/\mathrm{Nb}(72 \pm 5\,\text{Å})] \times 20$. However, because the neutron data were taken over a small region of q compared to the X-ray measurement, the neutron measurements are considerably less sensitive to the structural parameters than the X-ray measurements. Thus, we use the structural parameters derived from the X-ray results.

The magnetic contribution to the SPNR is demonstrated in Fig. 3(b) which shows the reflectivity difference between spin-up and spin-down divided by their average, $\Delta R/\bar{R}$. These data were modeled by including the London penetration length at the two surfaces of the multilayer and it is assumed that vortices are insignificant at this low field. Specifically, the magnetic field was taken to be

$$\vec{B}_L = \mu_o H \hat{x} \frac{\cosh(z/\lambda_L)}{\cosh(t/2\lambda_L)}, \tag{3.1}$$

where t is the total thickness of the multilayer sample and the applied field is along the x-axis. The solid curve is a best fit that gives $\lambda_L = 1800 \pm 200$ Å.

At higher magnetic field, the data were analyzed using a model assuming one and two rows of vortices. The magnetic field is given [2,13] by $\vec{B}(z) = \vec{B}_L(z) + \langle \vec{B}_V(y,z) \rangle$, where $\langle\,\rangle$ indicates an average over the in-plane y-coordinate and $\vec{B}_V$ is the magnetic field contribution from the vortices. Each vortex contributes a flux quantum, $\Phi_o = 2.067 \times 10^9\,\text{GÅ}^2$ so that the density of flux lines from $N+1$ vortices is,

$$\vec{\Phi} = \Phi_o \hat{x} \sum_{k=0}^{k=N} \delta(\vec{r} - \vec{r}_k), \tag{3.2}$$

where $\vec{r}_k$ is the location of kth vortex and the vortices are oriented along the applied field (the x-axis). The magnetic field at $r(y,z)$ in a thin film with thickness t due to N vortices including their images will be,

$$\vec{B}_V = \frac{\Phi_o \hat{x}}{2\pi\lambda_L^2} \sum_{k=-N/2}^{k=N/2} \sum_{n=-\infty}^{n=\infty} (-1)^n \times K_0\left(\frac{\sqrt{(z - nt - (-1)^n z_k)^2 + (y - y_k)^2}}{\lambda_L} \right), \tag{3.3}$$

where K_0 is a modified Bessel function of the zeroth order. Finally, $\vec{B}_V$ must be averaged over y in order to calculate the specular reflectivity, i.e.,

$$\langle \vec{B}_V \rangle = \frac{\Phi_o \hat{x}}{2l\lambda_L} \int_{-t/2}^{t/2} dz'\, D_V(z') \times \left\{ e^{-|z-z'|/\lambda_L} - e^{(2z-t)/2\lambda_L} \frac{\sinh[(2z'+t)/2\lambda_L]}{\sinh(t/\lambda_L)} + e^{-(2z+t)/2\lambda_L} \frac{\sinh[(2z'-t)/2\lambda_L}{\sinh(t/\lambda_L)} \right\} \tag{3.4}$$

where $1/l$ is the average linear density of vortices in the y-direction and $D_V(z)$ is a normalized distribution of vortices, $1 = \int_{-t/2}^{t/2} D_V(z')\,dz'$ in the z-direction. The average vortex density is then given as $n_0 = 1/lt$. The spatially varying one-dimensional

(1-D) magnetic field with vortices in a superconducting film can be obtained by summation of Eqs. (3.1) and (3.4).

Fig. 4 shows $\Delta R/\bar{R}$ measured at 2 K for ascending applied field: 1500 Oe (a), which is just above H_{c1}, and 2000 Oe (b), which is just below the first peak observed in Fig. 1. The data were analyzed for three vortex configurations: 1-row ($D_V(z)=\delta(z)$), 2-row ($D_V(z)=[\delta(z+t/6)+\delta(z-t/6)]/2$), and a uniform distribution ($D_V(z)=1/t$). Because of poorer statistics at high q where the reflectivity is weak, the data were fit up to $q<0.018\,\text{Å}^{-1}$. The vortex density was the only parameter varied and the results, along with the χ^2 of the fits, are given in Table 1 for each configuration and the corresponding curves are shown in Fig. 4. Generally, the 1-row of vortices fit only slightly better than the other configurations. Note that the determined vortex density is the same for the 1-row and 2-row configurations.

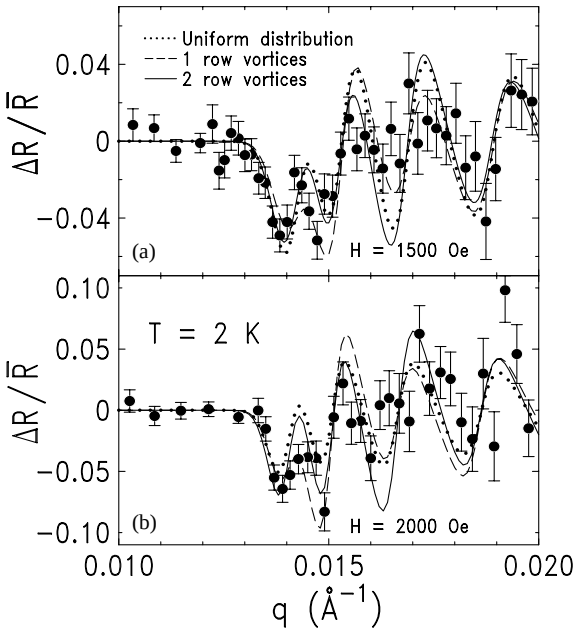

Fig. 4. $\Delta R/\bar{R}$ measured from the Nb(72 Å)/Al(20 Å) multilayer for ascending field at 2 K: (a) 1500 Oe and (b) 2000 Oe. The lines are a best fit assuming different distributions of vortices.

A measurement was also performed at 2000 Oe after cycling the field to 5400 Oe, as shown in Fig. 5(a). The same analysis was performed by comparing the three vortex distributions and, in

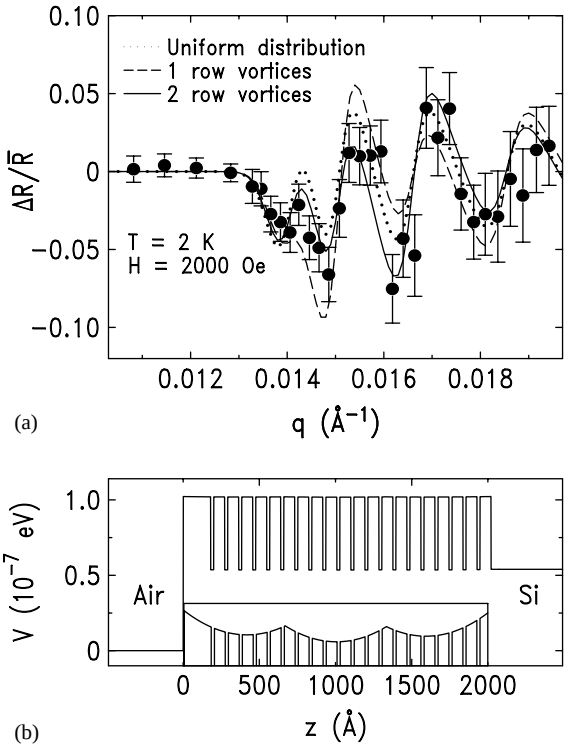

Fig. 5. (a) shows $\Delta R/\bar{R}$ measured from the Nb(72 Å)/Al(20 Å) multilayer at 2000 Oe (field-cycled) and 2 K. The lines are a best fit assuming different distributions of vortices. (b) shows the neutron scattering density profile that corresponds to 2 rows of vortices in (a). The inset shows a vertical expansion of the profile.

Table 1
Least-χ^2 fit to SPNR data with different vortex distributions

H(Oe)	1 row χ^2	Density (μm^{-2})	2 rows χ^2	Density (μm^{-2})	Uniform χ^2	Density (μm^{-2})
1500	2.788	30	2.974	30	3.499	35
2000	2.945	45	2.976	45	3.084	60
2000(cycled)	1.855	50	0.969	56	1.498	72

Table 2
Results of SPNR measurements and analysis with vortex rows

H (Oe)	Distribution	Density (μm^{-2})	$M_{\parallel}$ (G)
1500	1 row	30 ± 6	-51 ± 17
2000	1 row	45 ± 6	-57 ± 17
2000(cycled)	2 rows	56 ± 2	-42.5 ± 5

this case, the 2-row configuration gives a significantly better fit (see Table 1) than the other two. Fig. 5(b) shows the spin-up neutron potential that corresponds to the 2-row configuration given in (a). The results for the three measurements are summarized in Table 2, which also shows the parallel magnetization, $M_{\parallel}$, calculated [15] from the experimentally determined vortex density distribution.

A significant improvement in the quality of fit for *each* data set was obtained by using a model that assumes one row of vortices in the center of the sample but their position fluctuates about the center according to a Gaussian distribution, i.e., $D_V(z) = \alpha e^{-(\alpha z/W)^2}/\sqrt{\pi} W \mathrm{erf}(t\alpha/2W)$, where W is a full-width-at-half-maximum (FWHM) and $\alpha = 2\sqrt{\ln 2}$. Using Eq. (3.4), the 1-D magnetic field due to the vortices with a Gaussian distribution can be described as

$$\begin{aligned}\langle \vec{B}_V \rangle = &-\frac{\Phi_o \hat{x}}{4l\lambda_L} \frac{e^{-t/2\lambda_L + W^2/(2\alpha\lambda_L)^2}}{\mathrm{erf}(t\alpha/2W)} \frac{\cosh(z/\lambda_L)}{\cosh(t/2\lambda_L)} \\ &\times \left[\mathrm{erf}\left(\frac{\alpha}{W}\left[\frac{t}{2} - \frac{W^2}{2\alpha^2\lambda_L}\right]\right) + \mathrm{erf}\left(\frac{\alpha}{W}\left[\frac{t}{2} + \frac{W^2}{2\alpha^2\lambda_L}\right]\right)\right] \\ &+ \frac{\Phi_o \hat{x}}{4l\lambda_L} \frac{e^{W^2/(2\alpha\lambda_L)^2}}{\mathrm{erf}(t\alpha/2W)} \left\{ e^{-z/\lambda_L} \left[\mathrm{erf}\left(\frac{\alpha}{W}\left[\frac{t}{2} + \frac{W^2}{2\alpha^2\lambda_L}\right]\right)\right.\right. \\ &\left. + \mathrm{erf}\left(\frac{\alpha}{W}\left[z - \frac{W^2}{2\alpha^2\lambda_L}\right]\right)\right] \\ &+ e^{z/\lambda_L} \left[\mathrm{erf}\left(\frac{\alpha}{W}\left[\frac{t}{2} + \frac{W^2}{2\alpha^2\lambda_L}\right]\right)\right. \\ &\left.\left. - \mathrm{erf}\left(\frac{\alpha}{W}\left[z + \frac{W^2}{2\alpha^2\lambda_L}\right]\right)\right]\right\} \end{aligned} \quad (3.5)$$

where erf( ) is the error function. The fitted curves are shown in Fig. 6 and the results, along with the χ^2 values, are summarized in Table 3. It should be noted that the density and $M_{\parallel}$ are very similar to those obtained from the analysis of 1-row or 2-rows in Table 2. Thus, an essential conclusion is

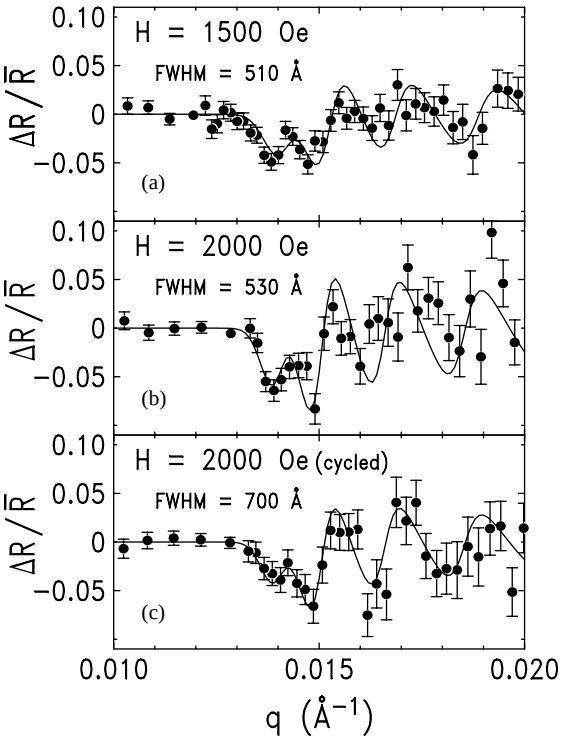

Fig. 6. $\Delta R/\bar{R}$ at 1500, 2000 Oe and (field-cycled) 2000 Oe. The solid lines are best fits to a Gaussian distribution of vortices.

that both ascending field measurements have a similar vortex distribution, differing only in density, and the vortices are *not* arranged in a perfect row. Rather, the vortices assume positions that fluctuate appreciably about the center with FWHM $\sim$ 500 Å, which is roughly 1/4 of the film thickness. A second conclusion is that the vortex distribution is different for the 2000 Oe cycled-field measurement. The distribution is clearly broader, with a FWHM $\sim$ 700 Å that is $\sim$1/3 of the film thickness, which is equal to the vortex row-spacing in the 2-row model. Thus, at the 2000 Oe cycled-field, it is not obvious whether the vortex distribution should be interpreted in terms of two rows of vortices or simply a more disordered distribution. Another question is whether the observed vortex distribution is, in fact, the vortex phase that occurs at a slightly higher applied field but "locked in" by hysteresis, or if it results from a mixed-phase that develops during the process of lowering the field. Hysteresis is evident in the

Table 3
Least-χ^2 fit with a Gaussian distribution of vortices

H (Oe)	χ^2	FWHM (Å)	Vortex density (μm^{-2})	$M_{\parallel}$ (G)	$\bar{M}$ (G)[a]
1500	2.056	510±51	33±3	−47±9	−66.6±7
2000	2.077	530±29	47±3	−58±9	−62.8±6
2000(cycled)	0.774	700±23	55±2	−42±6	83±8

[a] Magnetization was directly converted from the SQUID data in Fig. 8(a) (open circles) with no adjustable parameters.

values of the measured vortex density, which is slightly larger for the cycled field than for the virgin ascending field. The present experiment does, however, lend support to the assertions based on magnetization measurements from Nb/Cu multilayers [3] that vortices tend to the center of the film at low field and that the small peaks in the magnetization are associated with transitions in the shape of the vortex distribution. Future SPNR experiments will need to investigate higher applied fields as well as improve the counting statistics in order to fully understand the evolution of the vortex distribution.

4. Magnetization model

To assist with the interpretation of the experiments, we present a model calculation that minimizes the Gibbs free energy [2]:

$$G = G_0 + \frac{1}{\mu_o}\int_{V_S} dv\left\{\vec{\Phi}\cdot\left(\vec{B}_L + \frac{1}{2}\vec{B}_V\right)\right\}, \qquad (4.1)$$

where G_0 is the free energy for the system without vortices, μ_o is the permeability in vacuum, and V_S is the volume of the superconductor. In simplifying the free energy calculation, previous studies [4,19] have used an approximation for $\vec{B}_V$ which is valid only in the limit of $\lambda_L \gg$ the film thickness, t. Since this approximation is not applicable for our system where $\lambda_L \sim t$, we use Eq. (3.3) where we count term by term in the summation.

For the free energy calculation, we need two characteristic lengths, λ_L and the coherence length, ξ. $\lambda_L = 1800$ Å was determined from the SPNR measurement for the Nb(72 Å)/Al(20 Å) multilayer. The coherence length is related to the lower critical field, H_{c1}, when the applied field is parallel to the surface, which can be estimated from London theory [2,17,18]:

$$H_{c1} = \frac{\Phi_o}{4\pi\lambda_L^2}\frac{1}{1-\cosh(z/\lambda_L)/\cosh(t/2\lambda_L)} \times\left\{K_0\left(\frac{\xi}{\lambda_L}\right) + \sum_{n=-\infty, n\neq 0}^{\infty}(-1)^n \times K_0\left(\frac{|[1-(-1)^n]z - nt|}{\lambda_L}\right)\right\}, \qquad (4.2)$$

where we take $z = t/2 - \xi$, assuming that the free energy is zero at the surface when vortices first enter the superconductor. From our magnetization measurement we obtain $H_{c1} = 1200 \pm 200$ Oe and we calculate $\xi \sim 113$ Å.

Fig. 7 shows the minimum free energy calculated as a function applied magnetic field for the two vortex configurations: 1-row (dashed line) and 2-row (solid line), as shown in the lower inset. At a given field, the minimum free energy was determined by varying the density of vortices only. At small fields, the free energy of the system for 1-row is smaller than for 2-rows whereas above 2200 Oe the 2-row configuration minimizes the free energy—this agrees well with the first peak in the measured magnetization shown in Fig. 1. The inset at upper right corner of Fig. 7 shows the magnetization calculated for the global minimum free energy. There is the second transition (2-rows → 3-rows) at ~4000 Oe that also agrees well with the second peak observed in the measured M–H curve. In addition to matching the transition fields, the calculation also gives vortex densities that compare well with those measured by SPNR: the calculation yields 40 μm^{-2} at 1500 Oe, and 53 μm^{-2} at 2000 Oe as compared to ~30 μm^{-2} at

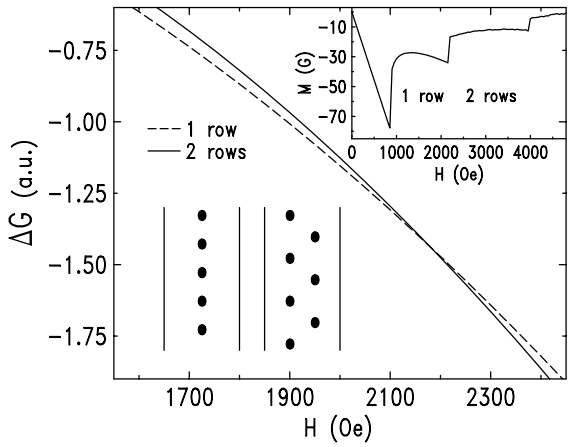

Fig. 7. Minimum Gibbs free energy calculated as a function of applied field assuming 1 row (dashed line) and 2 rows (solid line) of vortices. The location of the vortices for the two cases are shown in the lower-left inset. The upper-right inset shows the magnetization corresponding to the global minimum free energy.

1500 Oe, $\sim 45\,\mu m^{-2}$ at 2000 Oe, and $\sim 56\,\mu m^{-2}$ at cycled 2000 Oe from the SPNR measurement. The smaller measured vortex densities at ascending fields might be expected in the presence of surface barriers—kinetic barrier effects are not included in a calculation that minimizes the free energy. Similarly, we anticipate that the vortex row transition fields can be shifted to lower field values for a descending-field measurement, as has been experimentally observed by Sutton et al. [5].

5. Magnetization measurements at small tilted field

We investigated the magnetization for the field applied at a small angle with respect to the sample surface. As shown in Fig. 8, tilting the sample in the magnetic field allows vortices to enter the film at a lower value of applied field where the perpendicular component of the field circumvents the surface barrier and the critical field perpendicular to the surface, $H_{c1\perp}$, is reduced by the demagnetization effects of a thin-film sample geometry. Once flux enters the sample, peaks appear in the magnetization and the peak positions are listed in Table 4. For the Nb(72 Å)/Al(20 Å) sample at 2 K, peaks occur at 2250 Oe

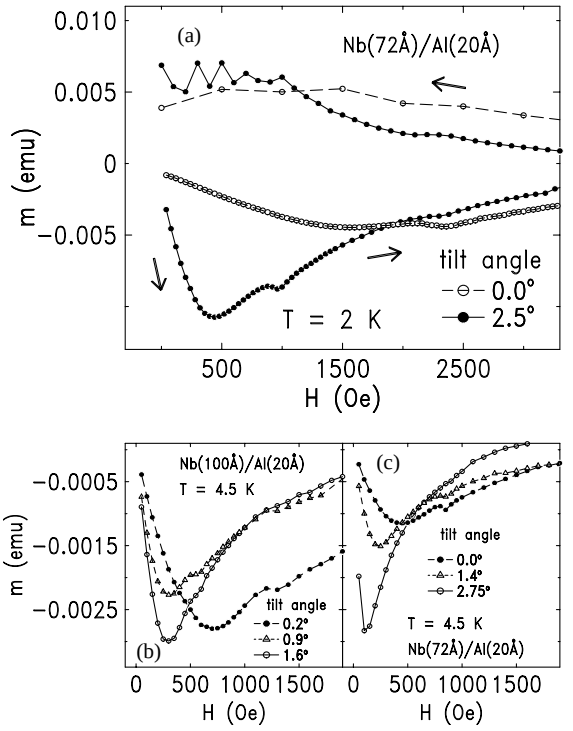

Fig. 8. Magnetic moments measured from Nb/Al multilayers at different tilt angles and temperatures. The arrows in (a) indicate the direction of measurement. Data of (b) and (c) were taken with increasing field. The lines are a guide to the eye.

(Fig. 8(a)) and at 3900 Oe (Fig. 1), independent of the tilt angle, and these positions agree well with those calculated in the inset of Fig. 7 for the transition between 1–2 rows and 2–3 rows, respectively. However, Fig. 8(a) shows that the peak at 950 Oe is observed only with a non-zero tilt angle. In the absence of a tilt, it is apparent from Fig. 8(a) that the surface barrier, which is ~ 1200 Oe, prevents flux from entering the sample. With a sufficient tilt, flux enters for $H \sin\theta > H_{c1\perp}$ (which is much smaller than $H_{c1\parallel}$ [20]) and we ascribe the transition at 950 Oe to $H_{c1\parallel}$ where it becomes energetically favorable for vortices to orient parallel to the film. We obtain $H_{c1\parallel} \sim 850$ Oe from the inset of Fig. 7 or equivalently by setting $z = 0$ in Eq. (4.2), which is in good agreement with the experimentally observed position. At 4.5 K, Fig. 8(c) shows that the surface barrier is lower and that this peak is observable without a tilt.

Table 4
Peak positions (Oe) in the SQUID magnetization

Configuration of multilayer			
Nb/[Al(20 Å)/Nb(72 Å)] × 20	950(2 K, 4.5 K)	2250(2 K, 4.5 K)	3900(2 K)
Nb/[Al(20 Å)/Nb(100 Å)] × 20	650(4.5 K)	1400(2 K, 4.5 K)	2450(2 K, 4.5 K)
Nb/[Al(20 Å)/Nb(130 Å)] × 20	1740(2 K)	2780(2 K)	

Similar results are observed in our measurements of Nb(100 Å)/Al(20 Å) at 4.5 K where all of the peaks shift to lower field values because of the combined effects of the larger total film thickness and the likely reduction in λ_L and increase of ξ. Since we do not have a measurement of λ_L in this case, we cannot make quantitative predictions for the fields of the transitions. We tentatively assign the peaks at 1400 and 2450 Oe (not shown) to the transition between 1–2 rows and 2–3 rows, respectively. With a non-zero sample tilt, we ascribe the peak at 650 Oe to the $H_{c1\|}$ transition, which is obscured by the surface barrier in the absence of a sample tilt. For the Nb(130 Å)/Al(20 Å) sample (Fig. 1) we observe two peaks which likely come from higher-order row-transitions, although, further investigations will be required to better characterize these.

Demagnetization effects play an important role in the magnetization measurements of thin-film superconductors. First, we show that the low-field SQUID magnetization data (Meissner regime, where the number of vortices is insignificant) can be quantitatively explained in terms of the demagnetization effects. The low-field slope of M vs. H was measured as a function of the tilt angle, θ, and, as shown in Fig. 9, these data are well described by the solid curves, which were fit to obtain the demagnetization factor, N, according to Ref. [15]:

$$4\pi M = -H\cos^2\theta\left\{1-\frac{2\lambda_L}{t}\tanh\left(\frac{t}{2\lambda_L}\right)\right\} - \frac{H\sin^2\theta}{1-N}. \quad (5.1)$$

For Nb(72 Å)/Al(20 Å), N is found to be 0.9986 ± 0.0011 at 2 K and 0.9935 ± 0.0007 at 4.5 K while it is 0.992 ± 0.0034 for Nb(100 Å)/Al(20 Å) at 4.5 K. These compare favorably with the calculated estimate of 0.994 for our sample geometry [21].

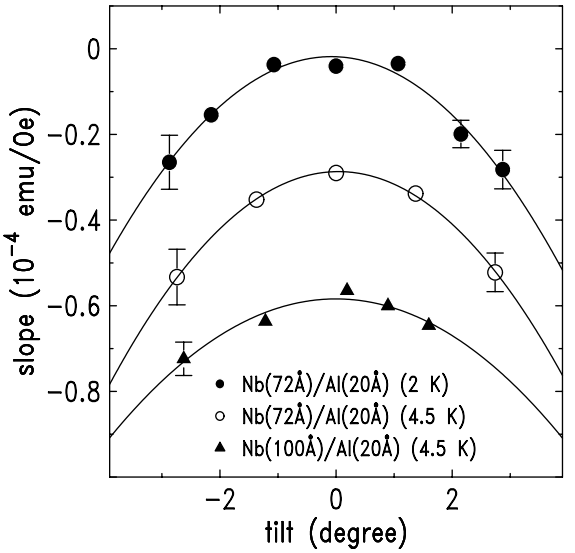

Fig. 9. The low-field slope of moment vs. field, obtained below H_{c1}, is plotted as a function of tilt angle. The solid lines are a best fit to Eq. (5.1). The data are shifted (open circle: -2.5×10^{-5}, and solid triangle: -5×10^{-5}) along the vertical axis for clarity.

At higher fields, the effects of demagnetization on the measured SQUID magnetization can be substantially larger [15] than in the Meissner regime if there is a component of vortex magnetic field that is perpendicular to the surface, $B_{V\perp}$, and we consider two implications for the present experiments. First, the lowest field transition at $H_{c1\|}$ corresponds to vortices that have components perpendicular to the surface and as H increases through $H_{c1\|}$ these vortices develop sections that become parallel to the surface and substantially elongate with increasing field. This undoubtedly affects $B_{V\perp}$, perhaps by reducing the number of

threading components of the vortices perpendicular to the surface, and this is the change that is detected by the SQUID magnetization. A second and important effect is that cycling the field leads to marked differences between the SPNR and SQUID measurements: the 2000 Oe field-cycled SPNR data is nearly reversible, with M being negative, whereas the field-cycled magnetization measured by the SQUID is, in fact, positive. This behavior is very similar to the observations in our previous studies of a Nb film [15], where a substantial $B_{V\perp}$ developed with decreasing applied field, corresponding to a rotation of B_V. Thus, we conclude that NbAl multilayers exhibit a similar reorientation of the vortex magnetic field as the applied field is removed.

6. Conclusions

The positions of peaks observed in the DC magnetization measured on Nb/Al multilayers were successfully predicted by energy minimization using only the λ_L measured by SPNR and the surface barrier field obtained from magnetization. These peaks correspond to transitions, driven by the interaction with the surface, between different numbers of vortex rows aligned with the surface. SPNR measurements at 1500 and 2000 Oe are consistent with a single row of vortices residing in the center of the film, although, an analysis with a Gaussian distribution suggests that the vortices exhibit substantial positional fluctuations, on the order of 1/4 of the film thickness. By considering a sample tilted in the applied field, a low-field peak in the DC magnetization was identified to correspond to the lower critical field parallel to the surface and the value of the transition field agrees well with the calculated value. Demagnetization effects are determined to be important in the magnetization measurements, permitting the perpendicular magnetization to be detected. By combining the SPNR and magnetization measurements, a reorientation of the vortex magnetic field was observed upon cycling the field, analogous to prior results on a pure Nb film and suggesting a surface-induced effect in addition to the row-transitions.

Acknowledgements

Support is gratefully acknowledged (P.F.M., S.W.H.) from the Midwest Superconductivity Consortium (MISCON) under DOE grant DE-FG02-90ER45427, the National Science Foundation under grant DMR96-23827, and the University of Missouri Research Board. The Intense Pulsed Neutron Source and work at Argonne National Laboratory is funded by the U.S. Department of Energy, BES-Materials Sciences, under Contract W-31-109-Eng-38. Research at Northwestern University is supported by the Northwestern Materials Research Center through the National Science Foundation-MRSEC program under grant DMR-9632472.

References

[1] C.P. Bean, J.D. Livingston, Phys. Rev. Lett. 12 (1964) 14.
[2] P.G. de Gennes, Superconductivity of Metals and Alloys, Addison-Wesley, New York, 1989; T.P. Orlando, K.A. Delin, Foundations of Applied Superconductivity, Addison-Wesley, New York, 1991.
[3] J. Guimpel, L. Civale, F. de la Cruz, J.M. Murduck, I.K. Schuller, Phys. Rev. B 38 (1988) 2342.
[4] S.H. Brongersma, E. Verweij, N.J. Koeman, D.G. de Groot, R. Griessen, B.I. Ivlev, Phys. Rev. Lett. 71 (1993) 2319.
[5] J. Sutton, Proc. Phys. Soc. 87 (1966) 791.
[6] P. Monceau, D. Saint-James, G. Waysand, Phys. Rev. B 12 (1975) 3673.
[7] T. Yamashita, L. Rinderer, J. Low Temp. Phys. 24 (1976) 695; N.Ya. Fogel, V.G. Cherkasova, Physica B 107 (1981) 291; P. Lobotka, I. Vávra, R. Senderák, D. Machajdík, M. Jergel, Š. Gaži, E. Rosseel, M. Baert, Y. Bruynseraede, M. Forsthuber, G. Hilscher, Physica C 299 (1994) 231.
[8] A. Pruymboom, P.H. Kes, E. van der Drift, S. Radelaar, Phys. Rev. Lett. 60 (1988) 1430.
[9] S.M. Yusuf, E.E. Fullerton, R.M. Osgood II, G.P. Felcher, J. Appl. Phys. 83 (1998) 6801.
[10] G. Hünnekes, H.G. Bohn, W. Schilling, H. Schulz, Phys. Rev. Lett. 72 (1994) 2271.
[11] M. Ziese, P. Esquinazi, P. Wagner, H. Adrian, S.H. Brongersma, R. Griessen, Phys. Rev. B 53 (1996) 8658.
[12] G.P. Felcher, R.T. Kampwirth, K.E. Gray, R. Felici, Phys. Rev. Lett. 52 (1984) 1539; H. Zhang, J.W. Lynn, C.F. Majkrzak, S.K. Satija, J.H. Kang, X.D. Wu, Phys. Rev. B 52 (1995) 10395; A. Mansour, R.O. Hilleke, G.P. Felcher, R.B. Lainbowitz, P. Chaudhari, S.S.P. Parkin, Physica B 156–157 (1989) 867; S.V. Gaponov, E.B. Dokukin, D.A. Korneev, E.B. Klyuenkov, W. Löbner, V.V. Pasyuk, A.V. Petrenko, Kh.

Rzhany, L.P. Chernenko, JETP Lett. 49 (1989) 316;
V. Lauter-Pasyuk, H.J. Aksenov, E.L. Kornilov, A.V. Petrenko, P. Leiderer, Physica B 248 (1998) 166.
[13] S.-W. Han, J.F. Ankner, H. Kaiser, E. Paraoanu, L.H. Greene, P.F. Miceli, Phys. Rev. B 59 (1999) 14692.
[14] V. Lauter-Pasyuk, H.J. Lauter, M. Lorenz, V.L. Aksenov, P. Leiderer, Physica B 267–268 (1999) 149.
[15] S.-W. Han, J. Farmer, P.F. Miceli, I.R. Roshchin, L.H. Greene, Phys. Rev. B 62 (2000) 9784.
[16] L.G. Parratt, Phys. Rev. B 95 (1954) 359;
S.K. Sinha, E.B. Sirota, S. Garoff, H.B. Stanley, Phys. Rev. B 38 (1988) 2297.
[17] A.A. Abrikosov, Fundamentals of the Theory of Metals, North-Holland, Amsterdam, 1988.
[18] S.-W. Han, Ph.D. Thesis, Department of Physics and Astronomy, University of Missouri-Columbia, 1998, unpublished.
[19] Gilson Carneiro, Phys. Rev. B 57 (1998) 6077;
Y. Mawatari, K. Yamafuji, Physica C 228 (1994) 336.
[20] L.N. Bulaevskii, M. Ledvij, V.G. Kogan, Phys. Rev. B 46 (1992) 366.
[21] D. Craik, Magnetism Principles and Applications, Wiley, New York, 1995, p. 298.